



Article

Influence of Slag-Based Geopolymer Concrete on the Seismic Behavior of Exterior Beam Column Joints

Settiannan Karuppanan Maniarsan ^{1,*}, Palanisamy Chandrasekaran ¹, Sridhar Jayaprakash ² 
and Gobinath Ravindran ³ 

¹ Department of Civil Engineering, Kongu Engineering College, Perundurai 638060, Tamil Nadu, India

² Department of Civil Engineering, GMR Institute of Technology, Razam 532127, Andhra Pradesh, India

³ Department of Civil Engineering, SR University, Warangal 506371, Telangana, India

* Correspondence: skmaniarasan@gmail.com

Abstract: In reinforced concrete (RC) constructions, the beam-column junctions are very sensitive to lateral and vertical loads. In the event of unforeseen earthquake and wind loads, this insufficient joint performance can lead to the failure of the entire structure. Cement industries emit a large amount of greenhouse gases during production, thus contributing to global warming. The nature of cement concrete is fragile. Cement output must be reduced in order to ensure environmental sustainability. Geopolymer concrete (GC), which is a green and low-carbon material, can be used in beam-column joints. M30 grade BBGC was developed and employed in the current study. Alkaline liquids are produced when sodium silicate and sodium hydroxide are mixed at room temperature. The alkaline liquid to fly ash ratio was fixed at 0.5, and the concentration of NaOH was fixed at 8 M. The mechanical properties of the Binary Blended Geopolymer concrete (BBGC), containing fly ash and GGBS, at proportions ranging from 0% to 100%, were investigated. This study was further expanded to examine the behavior of two groups of binary blended geopolymer concrete (BBGC) exterior beam-column joints, with cross sections of 230 mm × 120 mm and 170 mm × 120 mm. The column heights and lengths were both 600 mm under reverse cyclic loads in order to simulate earthquake conditions. The failure mechanism, ductility, energy absorption capacity, initial crack load, ultimate load carrying capacity, and structural performance was evaluated. The test findings showed that BBGC with 20% fly ash and 80% GGBS had the highest compressive strength and split tensile strength. When compared with other beam column joints, those containing 20% fly ash and 80% GGBS performed better under cyclic loading. The test findings imply that GGBS essentially enhances the joint performance of BBGC. The microstructural SEM and EDS studies revealed the reasons behind the improvement in strength of the GGBS fly ash-based Geopolymer concrete.

Keywords: geopolymer concrete; beam column joint; cyclic loading; GGBS; ductility; energy absorption; SEM



Citation: Maniarsan, S.K.; Chandrasekaran, P.; Jayaprakash, S.; Ravindran, G. Influence of Slag-Based Geopolymer Concrete on the Seismic Behavior of Exterior Beam Column Joints. *Sustainability* **2023**, *15*, 2327. <https://doi.org/10.3390/su15032327>

Academic Editor:
Constantin Chaliors

Received: 10 December 2022

Revised: 9 January 2023

Accepted: 18 January 2023

Published: 27 January 2023



Copyright: © 2023 by the authors. Licensee MDPI, Basel, Switzerland. This article is an open access article distributed under the terms and conditions of the Creative Commons Attribution (CC BY) license (<https://creativecommons.org/licenses/by/4.0/>).

1. Introduction

Geopolymer concrete (GC) is a modern form of concrete generated from industry waste. GC is being promoted as a viable alternative to traditional concrete, as well as a way to turn a number of waste streams into valuable by-products [1]. Geopolymer concrete also exhibits excellent compression strength, minimal creep, superior acid resistance, and low shrinking characteristics [2]. The curing process of geopolymer concrete has a significant impact on the formation of microstructures, and therefore, on the mechanical properties of geopolymer concrete [3]. The geopolymer's overall strength and fire resistance are influenced by the amount of fly ash in an alkaline solution. It was discovered that the strength of a fly ash-based geopolymer concrete increases with exposure to different temperatures. CO₂ emissions are lower in GC when compared with Ordinary Portland cement (OPC) [4–8]. Fly ash-based GC mixtures were mechanically enhanced, and the

C-S-H gel formation was enriched with the addition of 30% GGBS, as it resulted in denser microstructures in the geopolymer concrete [9]. The mechanical properties of geopolymer concrete reached their limit after interacting with specimens that contained 30% fly ash and 30% GGBS in an 8M sodium hydroxide solution [10]. Conventional concrete has a longer setting time, it is denser, and a greater level of drying shrinkage occurs than with Geopolymer Concrete (GPC). Although the GPC concrete had a significantly higher initial three-day strength than the OPC concrete, the compressive strength of the two concretes showed identical trends after 28 days [11]. The alkaline activator/fly ash ratio was found to have a significant impact on the compressive strength of the fly ash-based geopolymer. The alkaline activator/fly ash ratio of 0.4 was able to activate the geopolymerization of the fly ash more quickly than the other ratios [12]. Increasing the slag replacement levels, and reducing the alkaline activator concentration in Geopolymer concrete, reduces workability when the NaOH solution has a higher molarity; for instance, when $M = 14$. The increase in slag concentration from 10% to 50% resulted in a quick increase in compressive strength for the mixtures until 28 days, at which point, the pace of development decreased [13]. The inclusion of fly ash at 10%, in accordance with the weight of the cement in conventional concrete, increases the compressive strength, split tensile strength, and flexural strength by 19%, 46%, and 49% after 28 days of curing, respectively [14]. Geopolymer concrete with a higher NaOH molarity, when used as an alkaline activator, has a higher compressive strength; this has a major impact on the early strength of the concrete. The 1:1 ratio of NaOH and sodium silicate ($\text{SiO}_2/\text{Na}_2\text{O} = 8$) was found to initiate fly ash geopolymerization, and it achieved exceptional strength development, with a compressive strength of roughly 47 MPa [15]. The Geopolymer concrete achieves its desired strength significantly faster during heat curing than under normal curing conditions [16]. The compressive strength of a fly ash-based geopolymer is visibly affected by changes to the modulus and the doses of sodium silicate. When the modulus value was reduced and the sodium silicate dose was raised, the strength of the geopolymer samples rose. When the sodium silicate was activated, the strength reached an extreme value at a dose of 10%, and the strengths of the 3d, 7d, and 28d all exhibited similar trends [17]. The compressive strength of the geopolymer concrete treated with NaOH at 14M in a hot air oven had a strength that was roughly 10% greater than that of the steam-cured geopolymer concrete that was composed of a ternary mixture [18–21]. Geopolymer concrete containing pineapple fiber has a maximum flexural strength of 9.209 MPa and a compressive strength of 41.468 MPa, with a percentage of 0.50% at a concentration of NaOH 16 M [21]. The ternary blend geopolymer concrete beams containing fly ash, GGBS, Metakaolin with 1% steel fibers, and 0.1% polypropylene fibers showed an improvement in the first crack load and in the ultimate load, at 75% and 28%, respectively, when subjected to flexure, compared with conventional beams [22]. When compared with a control RC beam, an experimental evaluation of fiber-reinforced geopolymer concrete under monotonic loading revealed that it had superior engineering properties in terms of its modulus of elasticity, Poisson's ratio, and ductility ratio [23]. Reverse cyclic loading on geopolymer beam column joints showed that the first crack load and ultimate load is the same when compared with conventional RC beams. The energy absorption levels for the forward and reverse cycles were almost the same. Similarly, the ductility factor was 1.4% greater than the ductility factor for the conventional beam column joint [24]. The load deflection characteristics of the geopolymer reinforced beam column joint were better than those of the conventional concrete reinforced beam column joint. The geopolymer specimens showed a better performance under cyclic loading. The ultimate load for the geopolymer reinforced beam column joint increased by 32% compared with the conventional concrete reinforced beam column joint [25]. The anchoring performance of the reinforced Geopolymer external beam column joints improved as the development length of the beam flexural bars increased. Compared with typical RC beam column joints, the joint specimens had better energy dissipation capacity and fewer shear fractures [26]. The hybridization of fibers significantly improved the joint performance of the Ternary-mixed Geopolymer Concrete (TGPC) [27]. Due to the presence of steel, qualities associated

with a higher degree of strength were observed in GGBS–Dolomite geopolymer concrete, which demonstrated ductile behavior that was superior to cement concrete specimens. The introduction of steel fibers, with a 0.75% concrete volume, enhanced the ductility index by 73% [28]. Furthermore, the shear failure mode of the beam specimens in geopolymer concrete was changed to a more ductile mode with the insertion of fibers [29]. According to the test results, the cyclic behavior and fracture formation of the reinforced GC beam column joints differed from the RC beam column joints. With a joint shear demand-to-capacity ratio of 0.96–1.01, increasing the axial compression ratio increased the seismic performance of the reinforced GC beam column joints [30]. As the GC beam column joint increased the column's depth-to-beam rebar diameter ratio (h_c/db) from 21 to 25, the bond performance of the beam's flexural bars increased in the reinforced GC internal beam column joints, thus resulting in a significant increase in energy dissipation capacity [26]. When cyclic loading is applied to hybrid fiber-reinforced ternary blend geopolymer concrete (HTGPC) beam-column joints, they perform better in terms of ductility, energy absorption capacity, initial crack load, and peak load carrying capacity than traditional beam column joints. [31]. Fly ash and GGBS are intriguing materials in terms of their potential for sustainable development because their use in the alkali activation process does not require a great amount of energy; hence, the generation of harmful CO₂ emissions is decreased. The use of fly ash and GGBS in the alkali activation process (geopolymerization) also contributes to the reduction in natural raw material exploitation, and thus, it is possible to meet the more demanding needs of the construction industry in terms of the quality of construction materials [3]. The present study investigates the properties of GGBS fly ash-based Geopolymer concrete that contribute to its strength, as well as the effects of those properties. As industrial waste products, GGBS and fly ash were collected from steel mills and thermal plants. The GC mix design was created using a 'trial-and-error' process. Experimental studies were conducted on hardened geopolymer concrete with varying proportions of GGBS and fly ash, ranging from 0% to 100%. Moreover, based on the mechanical properties of GC, a combination of GC beam column joints comprising 80% GGBS, 20% fly ash, 100% fly ash, and 0% GGBS were employed to investigate their seismic performances. In order to conduct this investigation, Geopolymer Concrete beam column joints were placed onto two types of binary-blended geopolymer concrete (BBGC) exterior beam column joints, with cross sections of 230 mm × 120 mm and 170 mm × 120 mm. The column's height and length were both 600 mm. The structural performance was examined, including ductility and energy dissipation capability. Microstructural analyses via SEM, EDS, and other assessments were conducted for the 20% fly ash and 80% GGBS-based Geopolymer concrete to clarify the strength development mechanism of the hardened specimens.

2. Materials and Mixture Proportions

In this investigation, coarse particles of crushed stone aggregates, measuring 12.5 mm with a specific gravity of 2.75, were used. Moreover, sand derived from the riverbed, which complied with zone III regulations, and had a specific gravity of 2.52, were used as per the recommendations of IS 10262 2019 [31]. Class C fly ash, which passed through a 1.18 mm sieve, thus satisfying IS 2386(3)-1963 [32], was used. Sodium Silicate and Sodium Hydroxide were combined at room temperature to create the activated alkaline solution, which was then utilized to produce homogenous conditions. Pellets formed by Sodium Hydroxide were used, which had a purity rate of 97%. Moreover, Sodium Silicate, composed of SiO₂ and Na₂O (65%) and H₂O (35%), was also used. Indeed, a NaOH solution, with an 8 molar concentration has $8 \times 40 = 320$ g of NaOH solids per liter of water, where 40 denotes the molecular weight of NaOH. The chemical composition of the binders is shown in Table 1. It is worth noting that in both alkaline solutions, water plays a vital role. The sodium silicate and sodium hydroxide solutions were mixed for at least a day before the binder solution was added to the solid materials. The concrete mixture was designed in accordance with IS10262: 2019, in order to produce a M30 grade material. The concrete

mixture's proportions were 1:1.6:2.85 (The details of the mix proportion are available in the Supplementary Materials section). The mixture's requirements are shown in Table 2.

Table 1. Chemical composition of binders.

Binders	SiO ₂	Al ₂ O ₃	Fe ₂ O ₃	CaO	MgO	TiO ₂	SO ₃	LOI
Fly ash	65.6	28.0	3.0	1.0	1.0	0.5	0.25	0.29
GGBS	30.61	16.24	0.584	34.48	6.79	-	1.85	2.5

Table 2. Concrete Mixture's Proportions.

Mix Designation	Fly Ash (kg/m ³)	GGBS (kg/m ³)	Fine Aggregate (kg/m ³)	Coarse Aggregate (kg/m ³)	Na ₂ SiO ₃ (g/m ³)	NaOH (g/m ³)
GCF100G0	500	0	800	1425	180	72
GCF80G20	400	100	800	1425	180	72
GCF60G40	300	200	800	1425	180	72
GCF40G60	200	300	800	1425	180	72
GCF20G80	100	400	800	1425	180	72
GCF0G100	0	500	800	1425	180	72

First, fly ash, the fine aggregate, and the coarse aggregate were homogenized for approximately one minute under dry conditions. Next, to produce a homogenous combination, an alkaline solution, which was prepared one day prior to the casting, was added, and mixing continued for 2 min [33].

3. Experimental Investigation

3.1. Mechanical Properties of Concrete

The experimental inquiry entails casting concrete cubes, sized at 15 × 15 × 15 cm, and cylinders, sized at 30 × 15 cm, for each of the scenarios listed in Table 2. At 27 °C, the specimens were exposed to ambient curing. After 28 days of curing, the cast cubes were evaluated for compressive strength, and the cylinders were assessed for their split tensile strength under static loads. The compression strength analysis was performed in a compression machine with a load cell limit of 1000 kN. The split tensile strength of the concrete was ascertained by assessing the concrete cylinder sized at 30 × 15 cm, which was tested in a universal testing machine with a load cell limit of 1000 kN.

3.2. Flexural Behavior of the Beam Column Joints

3.2.1. Specimen Details

Exterior beam column joints, with Cross Sections of 230 mm × 120 mm and 170 mm × 120 mm, were employed for this investigation. The column's height and length are both 600 mm. Figure 1 depicts the reinforcing detail of the beam–column junction that was employed in the investigation. The junction was created using the strong column–weak beam design concepts. The beam was designed with 3 columns with 10 mm diameters in both the tension and compression zones; this acted as the main reinforcement and the spacing for the transverse reinforcement of the beam. For spans of up to 300 mm, a spacing of 30 mm c/c was given. For the remaining 150 mm, a spacing of 60mm c/c was given. For the longitudinal strengthening of the column, eight 8 mm diameter bars were used. Moreover, 6 mm diameter bars, with a spacing of 30 mm c/c at the midsection, and 60 mm c/c at the end of the column, were used as ties.

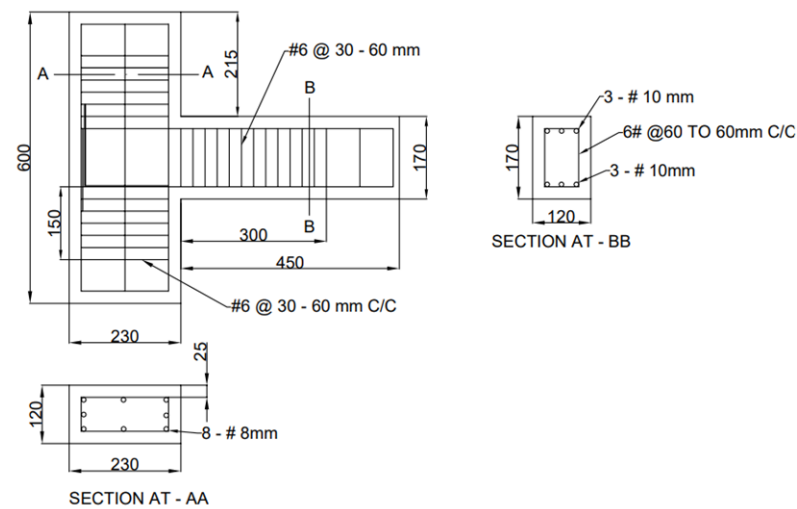


Figure 1. Reinforcement Details of the Beam Column Joint.

The samples were primarily intended to withstand seismic loads, in accordance with IS 1893 (Part I):2002 and IS13920:1993 [34] standards. To be favorable for the test facilities and loading arrangements, the specimen was scaled down to the 1/4th scale.

3.2.2. Casting and Curing of Specimens

Based on the mechanical qualities of concrete, the beam column joints were cast with 20% fly ash and 80% GGBS, which was found to be the best concrete combination. Using a concrete mixer, the fly ash and GGBS were first mixed with fine and coarse particles. The alkaline liquid was made by combining the sodium silicate solution with an 8 M sodium hydroxide solution 24 h before casting.

The alkaline liquid was poured into the mixer and vigorously mixed to create a homogeneous mixture. In order to condense the slurry, a needle vibrator was used. After 24 h of casting, the specimens were moved to a flat surface for air curing by using a plastic sheet, which was placed on top of the specimens. The concrete specimens were cured at room temperature, in the open, without exposure to sunshine. The specimens were placed in the shade for 28 days, in open air curing conditions. In the thin film wrap-up curing process, the concrete specimens were cured with plastic thin film sheets, which were wrapped around them. This ensured that the moisture content was captured inside the covers. The specimen was then exposed to sunlight for 28 days in an open area. Figure 2 depicts the curing of the BBGC beam column junction.



Figure 2. Curing of the Beam Column joint specimen.

3.2.3. Experimental Setup and Testing Procedure

To examine the beam column joints, a loading frame with a capacity of 100 tons was used, and the axial load was applied using a screw jack with a capacity of 50 tons. The load was applied at the end of the beam, cycled at regular intervals, and the deflection was measured under loaded conditions. The applied loads were recorded, and corresponding deflections were measured. Downward and upward displacements were measured using the Linear Variable Differential Transformer (LVDT) and dial gauges. The load setup of the beam column joint is shown in Figures 3 and 4.

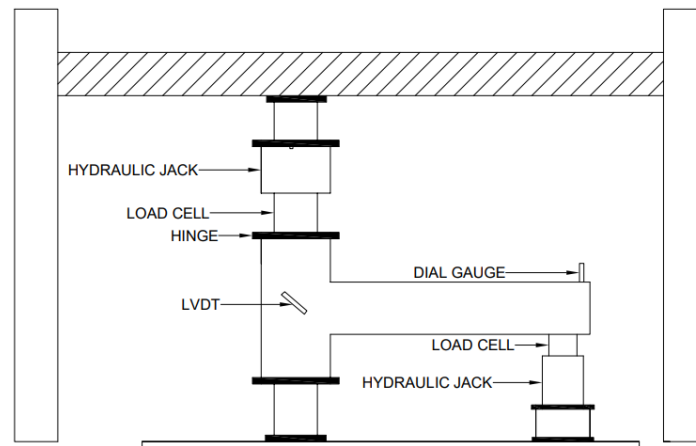
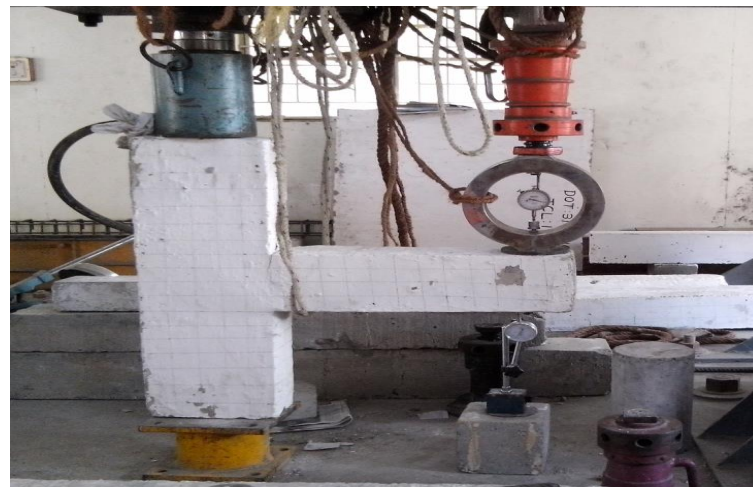


Figure 3. Schematic diagram of the test setup.



(a) Forward loading setup of the beam column joint.



(b) Reverse loading setup of the beam column joint.

Figure 4. Experimental test setup; **(a)** forward loading; and **(b)** reverse loading.

The specimens were bleached to enhance the visibility of the fracture patterns. Then, they were loaded at a particular point in the positive direction. To complete one cycle of reverse cycling loading, they were emptied in the other direction, at the same magnitude, and loaded again in the first position [32]. After each cycle, the degree of the stress increased, and this method was continued until the joints failed.

4. Results and Discussion

4.1. Compressive Strength

The effect of fly ash and GGBS integration on the compressive strength of concrete, with different quantities of fly ash and GGBS, was investigated. The compressive strength results, which were obtained with different percentages of fly ash and GGBS, after 28 days, were given in Figure 5. From the chart, it is evident that the maximum compressive strength was attained for GCF20G80, which achieved 41 N/mm^2 ; this is 54% higher than the results obtained for GCF100G0, which comprised 100% fly ash. Similarly, a rise in compressive strength for the concretes with 16%, 29%, 45%, and 47% fly ash was noted for GCF80G20, GCF60G40, GCF40G60, and GCF0G100, respectively. After 28 days of curing, the inclusion of GGBS increased the compressive strength; however, a higher proportion of fly ash decreased the compressive strength because it reduced the bond tension between the binder matrix and the aggregate [35]. Similar results were found in Mortar et al., where the compressive strength increased by 56% in the mixture containing 20% fly ash and 80% GGBS compared with the mixture containing 100% fly ash [36].

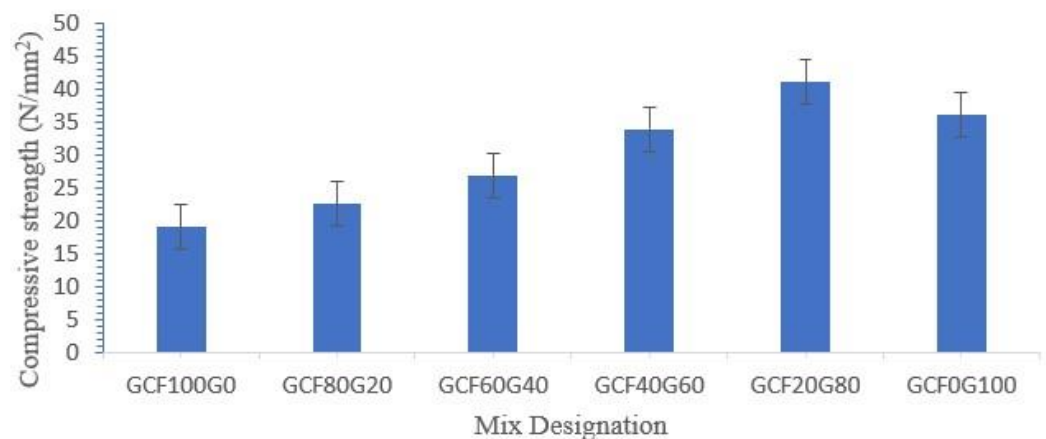


Figure 5. Compressive strength of the binary blend geopolymer concrete.

4.2. Split Tensile Strength

The effect of fly ash and GGBS on the split tensile strength of concrete was studied. Figure 6 shows the split tensile of concrete specimens, which were incorporated with different percentages of fly ash and GGBS. From the figure below, it is evident that the tensile strength of concrete improved with the addition of fly ash and GGBS; however, the incremental improvements in tensile strength stopped when the GGBS percentage was 100%. This is due to the fact that as the sand/ash ratio increased, the split tensile strength decreased. With regard to geopolymer concrete comprising 100% GGBS, similar results can be found in the work of Verma et al. [11] and Abdullah et al. [13]. The maximum split tensile strength obtained for GCF20G80 was 4.2 N/mm^2 , which was 60% higher than the tensile strength of GCF100G0. The split tensile strength of concrete improved as the GGBS content increased to 80%, beyond which, the tensile strength declined. In contrast to fly ash-based GC, fly ash GGBS-based Geopolymer concrete, combined with an alkaline solution, showed more substantial results after 28 days of ambient curing; this prompted the tensile strength to steadily decline [9].

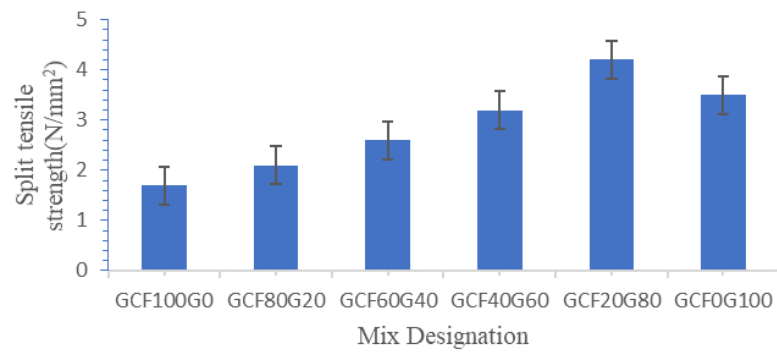


Figure 6. Split tensile strength of binary blend geopolymers concrete.

4.3. Beam Column Joints

The results of the cyclic loading test, which was performed on the GCF100G0 and GCF20G80 beam column joints that were subjected to film wrap-up curing, are shown in Figures 7 and 8. Loading was applied gradually, at 0, 4.5, 9, 13.5, 18, 22.5, 27 KN, and so on, in both forward and reverse directions, in incremental cycles, where the beam column joints took 22.5 KN of the ultimate load bearing capacity in the third cycle.

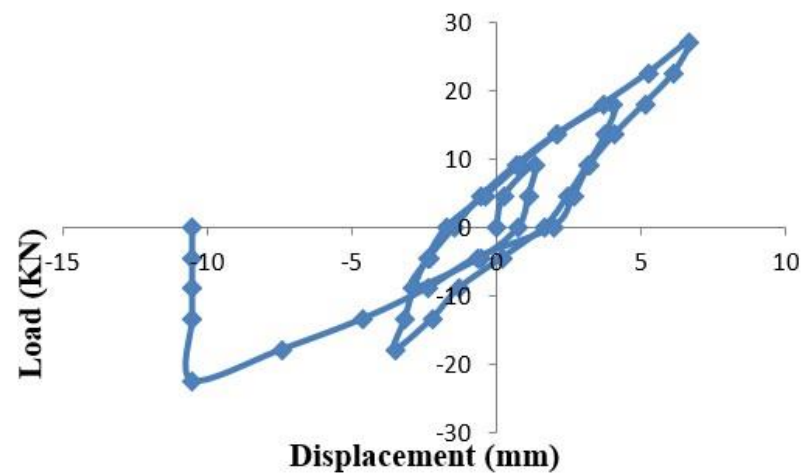


Figure 7. Load versus Deflection graph for the GCF100G0 beam column joint under Cyclic Loading conditions.

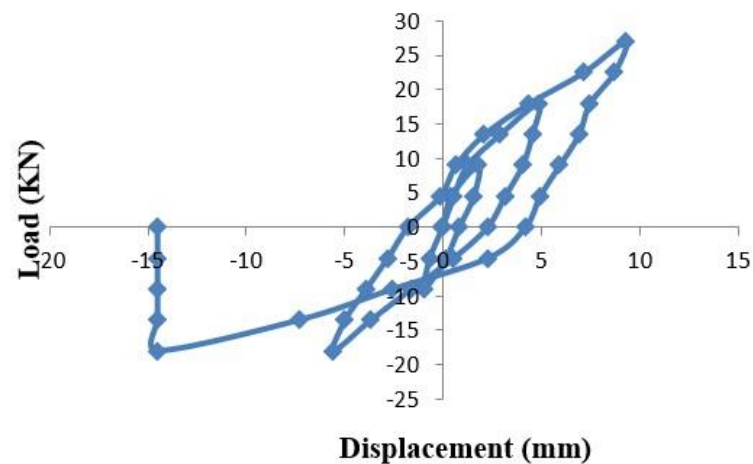


Figure 8. Load versus Deflection graph for the GCF20G80 beam column joint under Cyclic Loading conditions.

Figure 7 shows the load versus deflection of the GCF100G0 beam column joint under cyclic loading conditions. Initially, the load was applied in a forward direction, from 0 to 9 KN; then, the displacement measurements were noted. The load was then applied in the reverse direction, from 0 to 9 KN. The displacement measurements in the first cycle were low (i.e., 0, 1.33, 1.11, 0.77, -0.52 , -2.9 , -2.31 , and -1.43 mm). The second cycle load varied from 0 to 18 KN in both the forward and reverse loading directions; the displacement measurements in this cycle were -0.52 , 0.67, 2.07, 4.03, 3.77, 3.15, 2.47, 1.67, 0.22, -1.29 , -2.23 , -3.52 , -3.16 , -2.85 , -2.38 , and -1.7 mm, respectively. In the third cycle, the load varied from 0 to 27 KN in both the forward and reverse loading directions; the displacement measurements in this cycle were -0.4 , 0.8, 2.1, 3.7, 5.25, 6.66, 6.13, 5.13, 4.08, 3.22, 2.67, 1.97, -0.66 , -2.39 , -4.62 , -7.43 , and -10.51 mm. Here, the ultimate load carrying capacity of 27 KN in the forward loading direction, and -22.5 KN in the reverse loading direction, resulted in a specimen failure measurement of 10.51 mm.

Figure 8 shows the load versus deflection of the GCF20G80 beam column joint under cyclic loading conditions. Initially, the load was applied in the forward loading direction, from 0 to 9 KN; then, the displacement measurements were noted. The load was then applied in the reverse direction, from 0 to 9 KN. The displacement measurements in the first cycle were low (i.e., 0, 0.38, 1.78, 1.54, 0.8, 0.13, -0.99 , -0.69 , and -0.05 mm). The second cycle load varied from 0 to 18 KN in both the forward and reverse loading directions; the displacement measurements in this cycle were 0.53, 1.22, 2.88, 4.82, 4.52, 4.02, 3.13, 2.24, 0.52, -1.62 , -3.68 , -5.58 , -5 , -3.93 , -2.83 , and -1.81 mm, respectively. In the third cycle, the load varied from 0 to 27 KN in both the forward and reverse loading directions; the displacement measurements in this cycle were -0.16 , 0.64, 2.08, 4.35, 7.11, 9.24, 8.69, 7.44, 6.89, 5.91, 4.91, 4.17, 2.27, -2.58 , -7.31 , and -14.54 mm. Here, the ultimate load carrying capacity of 27 KN in the forward loading direction, and -18 KN in the reverse loading direction, resulted in a specimen failure measurement of 14.54 mm. A similar cyclical loading pattern was observed in Deepa Raj et al., wherein the geopolymer beam column had cross sections of 150 mm \times 200 mm and 200 mm \times 200 mm, for the beam and column, respectively [28].

The maximum load deflections of the GCF100G0 and GCF20G80 beam column joints, under forward and reverse cyclic loading conditions, are compared in Figure 9. With regard to the GCF100G0 specimen, it underwent three loading cycles to ensure that it could withstand the ultimate loading capacity of 27 KN. Furthermore, regarding the GCF20G80 specimen, the same process occurred to ensure that it could withstand the ultimate loading capacity of 27 KN in the third cycle. Comparing both specimens, the geopolymer concrete obtained slightly higher displacement measurements than the GCF100G0 specimen that underwent the same load pattern; however, it was also found to have a higher load carrying capacity after consecutive loading applications. The overall specimen failure measurements were found in the reverse loading direction in both cases. Similar load deflection characteristics were observed in the work of Saranya et al. [26], wherein the beam column joint had dimensions of 150 mm \times 200 mm for the beam and column, and the height of the column was 1000 mm.

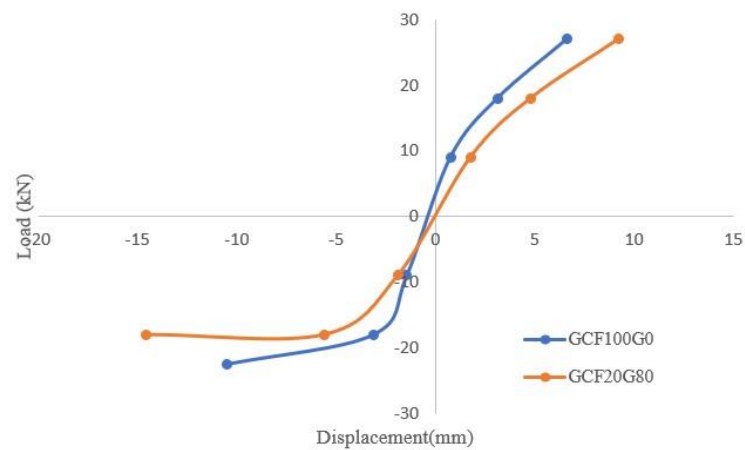


Figure 9. Comparison of Load versus Deflection graph and the GPC beam column joint.

4.4. Ductility

The ability of a structure to withstand further inelastic deformations, while preserving load resistance, is known as ductility. A quantitative measure of ductility must be based on a nearly horizontal load deformation response. The ratio of ultimate deformation to deformation at the start of the horizontal route (of first yield) may therefore be used to calculate ductility. This is illustrated in the load versus deflection diagram, shown in Figures 7 and 8. The ductility factor values for the various load cycles of the GCF100G0 and GCF20G80 beam column joints were calculated and are presented in Table 3. The table shows that the inclusion of 20% fly ash and 80% GGBS enhanced the ductility factor. As per the table, GCF20G80 had 22% higher ductility compared with GCF100G0. The results are similar to the findings of Saranya et al., which demonstrated that energy absorption increased by 18% for the beam column joint that included a geopolymer comprising 70% GGBS and 30% dolomite. The various cumulative ductility factors for all the cycles are shown in Figure 10.

Table 3. Test results of the beam column joints.

Mix Designation	First Crack Load (kN)	Ultimate Load Forward Cycle (kN)	Ultimate Load Reverse Cycle (kN)	Deflection at Ultimate Load Forward Cycle (kN)	Deflection at Ultimate Load Reverse Cycle (kN)	Ductility
GCF100G0	13.5	27	22.5	6.66	10.51	3.22
GCF20G80	13.5	27	18	9.24	14.54	4.49

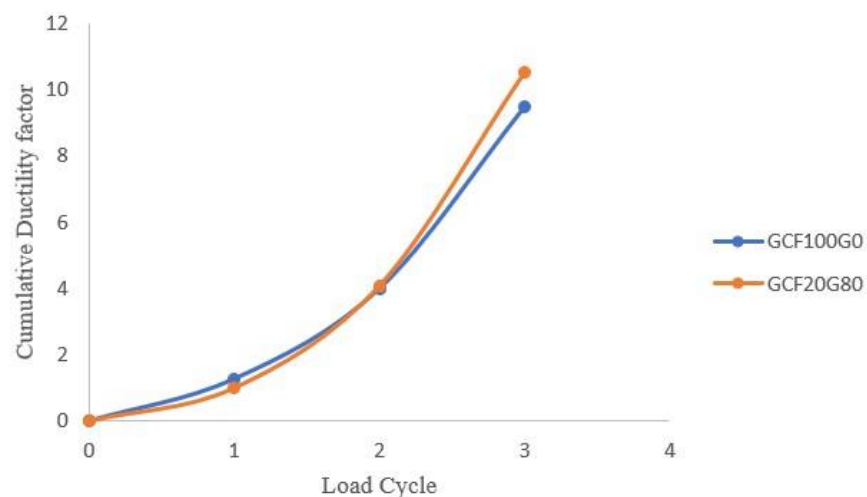


Figure 10. Cumulative ductility factor.

4.5. Energy Absorption Capacity

When the beam column junction is exposed to reverse cyclic loading (for instance, during a strong wind or an earthquake), some energy is absorbed in each load cycle. This energy absorption has the ability to strain or deform the structure to its limit of deflection. The total of the areas beneath the hysteric loops, from the load versus deflection diagram, was used to calculate the relative energy absorption capacities during various load cycles. Regarding GCF100G0, the cumulative energy absorbed during the first cycle of loading was calculated as 22 kNmm, and during the 3rd cycle of loading, it was calculated as 89 kNmm. Similarly, for GCF20G80, the energy absorption capacity was observed as being 25 kNmm and 107 kNmm for the first cycle and third cycle, respectively. The variations in the relative energy absorption capacity curve for all the cycles are shown in Figure 11.

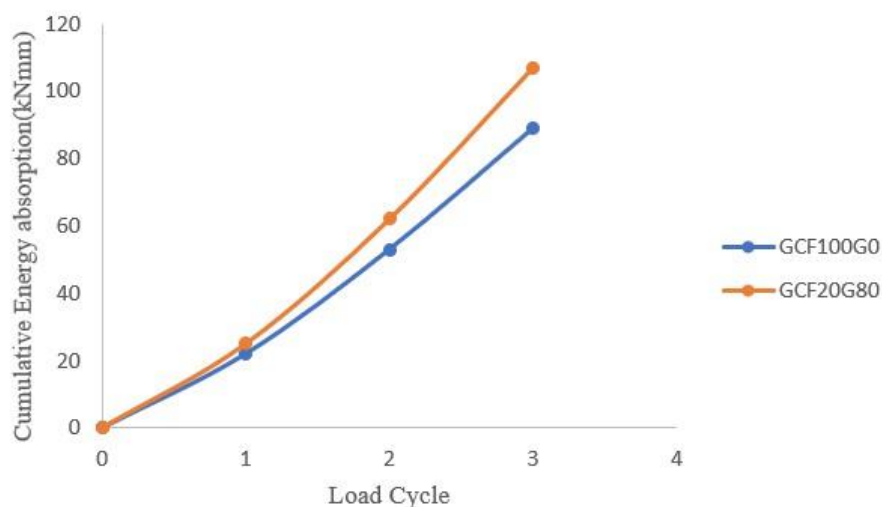


Figure 11. Cumulative energy absorption.

4.6. Mode of Failure

Forward and reverse cyclic loading tests were conducted on GCF100G0 and GCF20G80 using film wrap-up curing; then, the load deflection results were noted.

Figure 12 shows the initial cracks in the beam column joint. Initially, in the early stages of loading, no cracks were found until the second cycle, with regard to both the forward and reverse cycles. The first crack was found during forward loading cycle II, at 13.5 kN, at the top of the beam in the column joint, 450mm from the free end of the beam. Then, the cracks started to grow as the load increased, at the top and bottom of the beam's free end.



Figure 12. Initial cracks in the beam column joint.

The most common failures of the GCF100G0 and GCF20G80 beam column connectors can be seen in Figure 13. Regardless of the fly ash and GGBS concentration, both specimens created an initial fracture at the point where the beam and column met. When the load increased, the microcracks spread, and new cracks formed on the beam. The beam segment at the joint was riddled with fissures, and it collapsed as the fissures continued to grow. When compared with other GCF20F80 beam column junctions, the cracks in the GCF100G0 specimen were found to be more severe. No fractures were formed on the columns throughout the test, and no joint failure was observed in the tested specimens. This might be related to the fact that both the fly ash and GGBS may be responsible for fracture control. The energy absorption of a beam column junction can be enhanced by employing fly ash and GGBS [35]. Beam flexural failure occurred in the exterior beam column joint specimens, and the concrete was crushed at the beam plastic hinge zone. Similar observations may be found in Mao et al., wherein the beam column joint that included the geopolymer comprising 30% fly ash and 70% slag was used [26]. After comparing the load deflection envelope plot with the point where the curve's initial linearity diverged, the first fracture load was estimated.



Figure 13. Failure mode of the beam column joint.

4.7. SEM and EDS of Geopolymer Concrete

SEM and EDS investigations were performed on specimens containing fly ash and GGBS, as well as specimens which contained a combination of Sodium Silicate and Sodium Hydroxide, the latter of which acted as an alkaline activator. These investigations were conducted in order to detect the reactants of fly ash and GGBS, and to validate the interior microstructure. Figure 14 depicts SEM pictures of the microstructure of GCF20G80 after 28 days of flexure testing. Figure 14a demonstrates that geopolymerization occurred in the majority of the fly ash particles, thus suggesting the presence of C-S-H gels. The 20% fly ash and 80% GGBS mixture had a denser structure, comprising a thoroughly reacted matrix with few non-reacted fly ash particles. Non-reacted particles, it has been observed, do not function as 'fillers' in the mixture, but rather, they add to the strength of the mixture as it ages [9]. Figure 14b shows an enlarged image of the reactant on the fly ash surface. Reactants in the form of large prismatic cubes may be observed on the surface, as can the formation of countless little granule-shaped reactants.

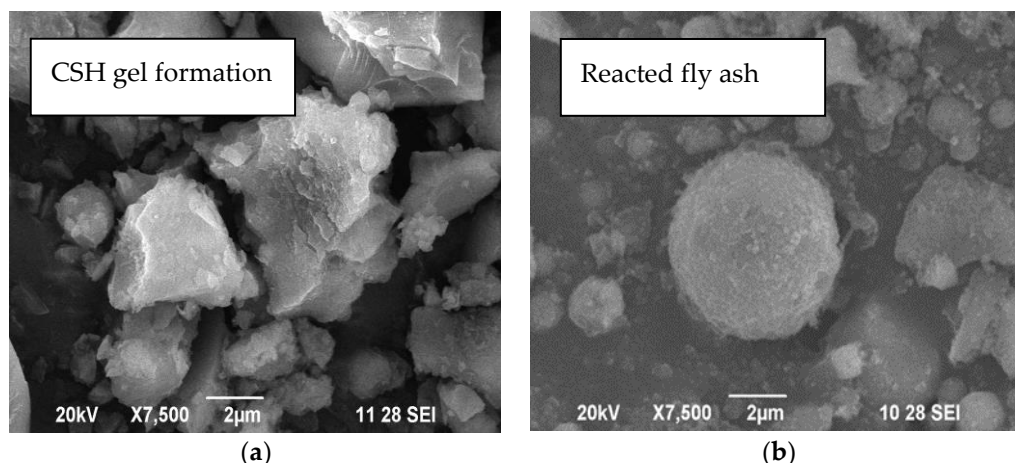


Figure 14. SEM images of fly ash and GGBS-based Geopolymer concrete; (a) CSH gel formation; and (b) reacted fly ash.

Figure 15 depicts the EDS analysis in relation to the SEM findings. It shows that the chosen positions include considerable amounts of 'Si,' 'Al,' 'Na,' and 'Ca.' The presence of Na can be explained by the creation of reactants during the geopolymerization condensation process. These reactants subsequently interact with the Na ions that have dissociated from the external NaOH, thus enabling the reactant products to agglomerate; this allowed the strength of the concrete to be built with fly ash particle combinations [15]. The EDS results demonstrate that the addition of fly ash to GGBS enhanced the flexural characteristics of Geopolymer Concrete.

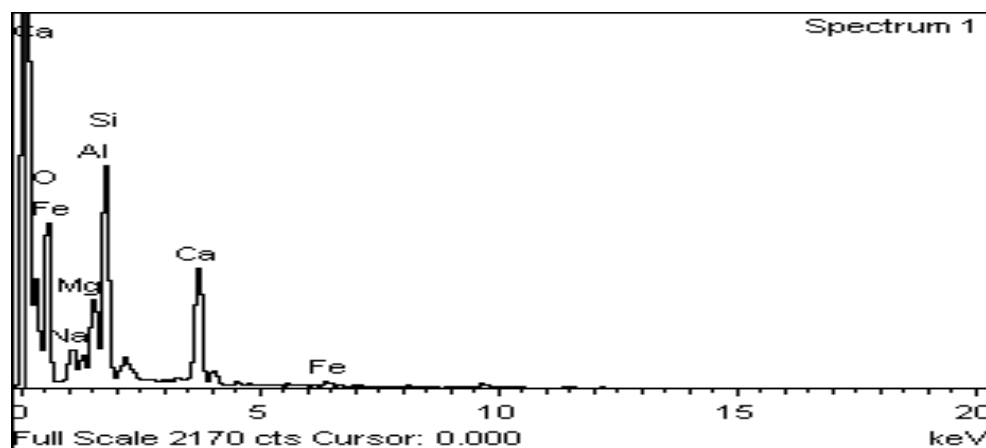


Figure 15. EDS images of fly ash and GGBS based Geopolymer concrete.

5. Conclusions

This experimental investigation has led to the following conclusions:

1. The maximum compressive strength and split tensile strength were obtained for GCF20G80; they were 54% and 60% higher than GCF100G0, respectively.
2. The addition of fly ash and GGBS increased the ultimate strength, ductility, and energy dissipation capability. This demonstrates that binary blend geopolymer concrete may be utilized efficiently in beam column joints.
3. The ductility factor for the beam column joint, with 20% fly ash and 80% GGBS (GCF20G80), had 22% higher ductility compared with the beam column joint comprising 100% fly ash.
4. The cumulative energy dissipation of the GCF20G80 was improved by a maximum of 16.8% compared with the cumulative energy dissipation of the GCF100G0 specimen.

5. Numerous cracks were identified in the GCF20G80 specimens, and the width of cracks was observed to be higher in the GCF100G0 specimens than the GCF20G80 specimens.
6. It was found that by adding 80% GGBS to fly ash-based Geopolymer concrete, the mechanical characteristics of the concrete improved, and the production of the C-S-H gel increased, thus resulting in denser microstructures.
7. SEM and EDS pictures demonstrate that the Geopolymer is tightly packed, and it has fewer pores; the pictures show that a partial replacement of fly ash with GGBS enhanced the mechanical characteristics of the GC. This was primarily caused by the production of additional geopolymeric gels.
8. The microstructural study revealed that there were other crystalline state developments arising from different components, including Si, Ca, Al, and Na.
9. A binary mixture of geopolymer concrete can be used as a superior alternative to traditional cement concrete for constructions that must withstand unforeseen events, such as earthquakes and wind stresses.
10. By focusing on critical role areas, this report illuminated a path ahead for further research and the development of GC in the construction field. The use of GC will result in the sustainable utilization of industrial byproducts, and it can be employed as a novel cementitious material that produces lower CO₂ emissions than standard concrete. More research on commercially accessible activator solutions is required to manufacture large quantities of GC and apply it to all 'ready-mix' concrete plants. The studies recommend using less than 20% fly ash for fly ash-GGBS-based GC.

Supplementary Materials: The following are available online at <https://www.mdpi.com/article/10.3390/su15032327/s1>. Annexure I. Mix Design for M30 Grade of Geopolymer Concrete.

Author Contributions: Conceptualization, S.K.M. and P.C.; Data curation, S.J. and G.R.; Investigation, S.K.M.; Methodology, S.K.M. and P.C.; Project administration, S.K.M.; Resources, P.C.; Software, S.J.; Writing original draft, S.K.M., S.J. and G.R.; Writing—review & editing, S.K.M., S.J. and G.R.; All authors have read and agreed to the published version of the manuscript.

Funding: This research received no external funding.

Institutional Review Board Statement: Not applicable.

Informed Consent Statement: Not applicable.

Data Availability Statement: No data, models or code were generated or used during the study.

Conflicts of Interest: The authors declare no conflict of interest.

References

1. McLellan, B.C.; Williams, R.P.; Lay, J.; Van Riessen, A.; Corder, G.D. Costs and carbon emissions for geopolymer pastes in comparison to ordinary portland cement. *J. Clean. Prod.* **2011**, *19*, 1080–1090. [[CrossRef](#)]
2. Garcia-Lodeiro, I.; Palomo, A.; Fernández-Jiménez, A. Alkali—Aggregate reaction in activated flyash systems. *Cem. Concr. Res.* **2007**, *37*, 175–183. [[CrossRef](#)]
3. Komljenović, M.; Baščarević, Z.; Bradić, V. Mechanical and microstructural properties of alkali-activated flyash geopolymers. *J. Hazard. Mater.* **2010**, *181*, 35–42. [[CrossRef](#)] [[PubMed](#)]
4. Kong, D.L.Y.; Sanjayan, J.G. Damage behavior of geopolymer composites exposed to elevated temperatures. *Cem. Concr. Compos.* **2008**, *30*, 986–991. [[CrossRef](#)]
5. Turner, L.K.; Collins, F.G. Carbon dioxide equivalent (CO₂-e) emissions: A comparison between geopolymer and OPC cement concrete. *Constr. Build. Mater.* **2013**, *43*, 125–130. [[CrossRef](#)]
6. Van Deventer, J.S.J.; Provis, J.L.; Duxson, P. Technical and commercial progress in the adoption of geopolymer cement. *Miner. Eng.* **2012**, *29*, 89–104. [[CrossRef](#)]
7. Okoye, F.N. Geopolymer binder: A veritable alternative to Portland cement. *Mater. Today Proc.* **2017**, *4*, 5599–5604. [[CrossRef](#)]
8. Maniarsan, S.K.; Kumar, V.S.; Chandrasekaran, P. Fly ash Based Self-Cleaning Geopolymer Concrete Using Nanotechnology-A Review. *Int. J. Sci. Technol. Res.* **2017**, *9*, 1631–1639.
9. Bellum, R.R.; Muniraj, K.; Madduru, S.R.C. Influence of activator solution on microstructural and mechanical properties of geopolymer concrete. *Materialia* **2020**, *10*, 100659. [[CrossRef](#)]

10. Ashveenkumar, P.; Preethi, M.; Prashanth, P. Mechanical properties of geopolymer concrete with varying cement content using flyash and ground granulated blast furnace slag. *Int. J. Eng. Sci. Technol.* **2021**, *13*, 57–64. [[CrossRef](#)]
11. Verma, M.; Upreti, K.; Vats, P.; Singh, S.; Mishra, D.K.; Tiwari, B. Experimental Analysis of Geopolymer Concrete: A Sustainable and Economic Concrete Using the Cost Estimation Model. *Adv. Mater. Sci. Eng.* **2022**, *2022*, 16. [[CrossRef](#)]
12. Al Bakri Abdullah, M.M.; Kamarudin, H.; Abdulkareem, O.A.K.A.; Ghazali, C.M.R.; Rafiza, A.R.; Norazian, M.N. Optimization of alkaline activator/flyash ratio on the compressive strength of manufacturing fly ash-based geopolymer. *Appl. Mech. Mater.* **2012**, *110*, 734–739.
13. Waqas, R.M.; Butt, F.; Zhu, X.; Jiang, T.; Tufail, R.F. A Comprehensive Study on the Factors Affecting the Workability and Mechanical Properties of Ambient Cured Flyash and Slag Based Geopolymer Concrete. *Appl. Sci.* **2021**, *11*, 8722. [[CrossRef](#)]
14. Sridhar, J.; Jegatheeswaran, D.; Dash, B. Mechanical Properties of Latex Modified Nylon Fibre Reinforced Concrete with Partial Replacement of Cement by Flyash. *Eco. Env. Con.* **2022**, *11*, S164–S169. [[CrossRef](#)]
15. Ryu, G.S.; Lee, Y.B.; Koh, K.T.; Chung, Y.S. The mechanical properties of flyash-based geopolymer concrete with alkaline activators. *Constr. Build. Mater.* **2013**, *47*, 409–418. [[CrossRef](#)]
16. Ramujee, K.; PothaRaju, M. Mechanical properties of geopolymer concrete composites. *Mater. Today Proc.* **2017**, *4*, 2937–2945. [[CrossRef](#)]
17. Lv, Q.; Yu, J.; Ji, F.; Gu, L.; Chen, Y.; Shan, X. Mechanical Property and Microstructure of Flyash-Based Geopolymer Activated by Sodium Silicate. *KSCCE J. Civ. Eng.* **2021**, *25*, 1765–1777. [[CrossRef](#)]
18. Kumar, V.S.; Ganesan, N.; Indira, P. Effect of molarity of sodium hydroxide and curing method on the compressive strength of ternary blend geopolymer concrete. *IOP Conf. Ser. Earth Environ. Sci.* **2017**, *80*, 12011. [[CrossRef](#)]
19. Karuppanan, M.S.; Palanisamy, C.; Farook, M.S.M.; Natarajan, M. Study on flyash and GGBS based oven cured geopolymer concrete. *AIP Conf. Proc.* **2020**, *2240*, 60001.
20. Sharmila, S.; Maniarasan, S.; Venkatachalam, S. Experimental Study on Strength Assessment of Flyash based Geopolymer Matrix. *Int. Res. J. Eng. Technol.* **2019**, *6*, 989–993.
21. Zulfiati, R.; Idris, Y. Mechanical properties of flyash-based geopolymer with natural fiber. *J. Phys. Conf. Ser.* **2019**, *1198*, 82021. [[CrossRef](#)]
22. Kumar, V.S.; Ganesan, N.; Indira, P.V.; Murali, G.; Vatin, N.I. Flexural Behaviour of Hybrid Fibre-Reinforced Ternary Blend Geopolymer Concrete Beams. *Sustainability* **2022**, *14*, 5954. [[CrossRef](#)]
23. Saranya, P.; Nagarajan, P.; Shashikala, A.P. Performance evaluation of geopolymer concrete beams under monotonic loading. *Structures* **2019**, *20*, 560–569. [[CrossRef](#)]
24. Raj, S.D.; Ganesan, N.; Abraham, R.; Raju, A. Behavior of geopolymer and conventional concrete beam column joints under reverse cyclic loading. *Adv. Concr. Constr.* **2016**, *4*, 161. [[CrossRef](#)]
25. Kumar, P.; Mahakavi, P.; Priya, S. Experimental Study on Structural Behaviour of Beam Column Joint Using Geo-Polymer Concrete. *Int. J. Civ. Eng. Technol.* **2017**, *8*, 688.
26. Mao, Y.; Hwang, H.-J.; Du, Y.; Su, J.; Hu, X.; Liu, Y.; Shi, C. Bond and anchorage performance of beam flexural bars in beam-column joints using slag-based geopolymer concrete and their effect on seismic performance. *Eng. Struct.* **2022**, *273*, 115062. [[CrossRef](#)]
27. Kumar, V.S.; Ganesan, N.; Indira, P.V.; Murali, G.; Vatin, N.I. Behaviour of Hybrid Fibre-Reinforced Ternary Blend Geopolymer Concrete Beam-Column Joints under Reverse Cyclic Loading. *Polymers* **2022**, *14*, 2239. [[CrossRef](#)]
28. Saranya, P.; Nagarajan, P.; Shashikala, A.P. Seismic performance of geopolymer concrete beam-column joints under reverse cyclic loading. *Innov. Infrastruct. Solut.* **2021**, *6*, 1–10. [[CrossRef](#)]
29. Raj, S.D.; Ramachandran, A. Performance of hybrid fibre reinforced geopolymer concrete beams. *SN Appl. Sci.* **2019**, *1*, 1–8.
30. Mao, Y.; Du, Y.; Hwang, H.; Su, J.; Hu, X.; Liu, Y.; Shi, C. Seismic performance of interior beam-column joints using reinforced slag-based geopolymer concrete. *Earthq. Eng. Struct. Dyn.* **2022**, *52*, 285–307. [[CrossRef](#)]
31. IS 10262; Concrete Mix Proportioning-Guidelines. Bureau of Indian Standards: New Delhi, India, 2019.
32. IS 2386 (Part III); Methods of Test for Aggregates for concrete, Part 3 Specific Gravity, Density, Voids, Voids, Absorption and Bulking. Bureau of Indian Standards: New Delhi, India, 1963.
33. Anuradha, R.; Sreevidya, V.; Venkatasubramani, R.; Rangan, B.V. Modified guidelines for geopolymer concrete mix design using Indian standard. *Asian J. Civ. Eng.* **2012**, *13*, 353–364.
34. IS 13920; Ductile Detailing of Reinforced Concrete Structures Subjected to Seismic Forces: Code of Practice. Bureau of Indian Standards: New Delhi, India, 1993.
35. Shariq, M.; Prasad, J.; Masood, A. Effect of GGBFS on time dependent compressive strength of concrete. *Constr. Build. Mater.* **2010**, *24*, 1469–1478. [[CrossRef](#)]
36. Nurul Aida Mohd Mortar; Kamarudin, H.; Rafiza, R.A.; Meor, T.; Rosnita, M. Compressive Strength of Fly Ash Geopolymer Concrete by Varying Sodium Hydroxide Molarity and Aggregate to Binder Ratio. *IOP Conf. Ser. Mater. Sci. Eng.* **2020**, *864*, 012037. [[CrossRef](#)]

Disclaimer/Publisher’s Note: The statements, opinions and data contained in all publications are solely those of the individual author(s) and contributor(s) and not of MDPI and/or the editor(s). MDPI and/or the editor(s) disclaim responsibility for any injury to people or property resulting from any ideas, methods, instructions or products referred to in the content.